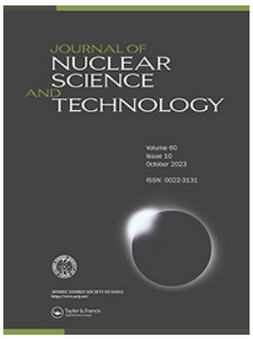

Journal of Nuclear Science and Technology

ISSN: (Print) (Online) Journal homepage: https://www.tandfonline.com/loi/tnst20

A membrane, pseudo-vertical p-i-n diamond detector

Tetsuichi Kishishita, Kimiyoshi Ichikawa, Kazuya Tauchi, Masayoshi Shoji, Masayuki Hagiwara, Satoshi Koizumi & Manobu M. Tanaka

To cite this article: Tetsuichi Kishishita, Kimiyoshi Ichikawa, Kazuya Tauchi, Masayoshi Shoji, Masayuki Hagiwara, Satoshi Koizumi & Manobu M. Tanaka (2023) A membrane, pseudo-vertical p-i-n diamond detector, Journal of Nuclear Science and Technology, 60:10, 1285-1291, DOI: 10.1080/00223131.2023.2190548

To link to this article: https://doi.org/10.1080/00223131.2023.2190548

© 2023 The Author(s). Published by Informa UK Limited, trading as Taylor & Francis Group.

Published online: 03 Apr 2023.

Submit your article to this journal

Article views: 598

View related articles

View Crossmark data

Full Terms & Conditions of access and use can be found at
https://www.tandfonline.com/action/journalInformation?journalCode=tnst20

JOURNAL OF NUCLEAR SCIENCE AND TECHNOLOGY
2023, VOL. 60, NO. 10, 1285–1291
https://doi.org/10.1080/00223131.2023.2190548

ARTICLE

OPEN ACCESS Check for updates

A membrane, pseudo-vertical p-i-n diamond detector

Tetsuichi Kishishita[a], Kimiyoshi Ichikawa[b], Kazuya Tauchi[a], Masayoshi Shoji[a], Masayuki Hagiwara[c], Satoshi Koizumi[b] and Manobu M. Tanaka[a]

[a]KEK, High Energy Accelerator Research Organization, Institute of Nuclear and Particle Studies, Tsukuba, Ibaraki, Japan; [b]National Institute for Materials Science, Tsukuba, Ibaraki, Japan; [c]National Institutes for Quantum Science and Technology, Sendai, Miyagi, Japan

ABSTRACT

We report on the membrane diamond detector, which consists of 5 μm-thick p-i-n diodes and a dedicated front-end ASIC, fabricated in a 65-nm CMOS technology. The p-i-n diode has an attractive feature for low γ-ray sensitivities due to its extremely thin drift layer, which is difficult to form by etching of bulk diamond with a Metal–Insulator–Metal structure. The pseudo-vertical p-i-n diode structure was formed on the single crystal diamond {111} substrate by MPCVD and dry-etching process. The readout electronics was designed to meet specifications for real-time neutron monitoring in harsh γ-ray environments. The prototype system was evaluated in charge distribution measurements induced by α-particles from ^{241}Am. The charge spectra were successfully obtained from multi-channels, each of which has a diameter of 250 μm aligning in a pixel matrix. By combining with neutron converters, *e.g.* ^{10}B or ^{7}Li, we expect the detector system as a good candidate for detecting spontaneous fission neutrons, emitted from submerged fuel debris at the Fukushima Daiichi Nuclear Power Plant in Japan.

ARTICLE HISTORY
Received 2 November 2022
Accepted 22 February 2023

KEYWORDS
Nuclear power plant; alpha particle; gamma ray

1. Introduction

Diamond has been considered as a potential alternative to conventional gas-filled neutron sensors such as BF_3 proportional counters, by virtue of the compactness and high signal-to-noise ratio owing to its wide bandgap property. Slow neutrons are detected by attaching converters such as $^{10}B_2O_3$ or ^{6}LiF onto a diode surface or contact metals. The most common reaction $^{10}_{5}\mathrm{B} + n \rightarrow ^{4}_{2}\mathrm{He}(1.47\mathrm{MeV}) + ^{7}_{3}\mathrm{Li}(0.84\mathrm{MeV})$ produces a sufficiently large amount of charge signals (≈ 100 ke$^-$) in diamonds, and almost 100% charge-collection efficiency (CCE) with an energy resolution of $< 1\%$ was reported in the past study [1].

Current structures of diamond radiation sensors are concentrated on a Metal–Insulator-Metal (MIM) with the Schottky barrier surface at the metal–diamond interface. In this configuration, high-purity diamond plates are sandwiched with parallel electrodes. The sensor requires an electric field of several kV/cm to 10 kV/cm to obtain the full CCE.

To reduce reverse bias voltages, new sensor structures are proposed such as membrane detectors or Metal–Insulator–Semiconductor (MIS) structures by reduction in the drift length of the charge carrier [2,3]. These thin sensors are expected to be more efficient thermal neutron detection due to the higher γ-ray rejection capability [4].

As extremely thin devices, the pn junctions or p-i-n diodes provide a unique feature, which is difficult to form merely by etching of bulk diamond; since the built-in potential (V_{bi}) of the pn junction is more than twice those of typical diamond Schottky barrier diodes, it forms a field sufficient to transport charges created by radiation when the drift layer thickness is several micrometers. Small sensors without a bias voltage power supply are also expected using the pn junction. Thus, the excellent radiation durability of diamond material, high count rate capabilities with potentially segmented channels, *e.g.* small pixel diodes, and low γ-ray sensitivity with the membrane structure are drawing more attention in the field of nuclear applications, especially as real-time radiation monitors at the Fukushima Daiichi Nuclear Power Plant (NPP) in Japan [5].

Figure 1 (left) shows a 3D image of the expected flooded primary containment vessel at the Fukushima NPP. The urgent task is the localization and characterization of the fuel debris in the flooded primary containment vessel (PCV) on-site. This is achievable by detecting spontaneous fission neutrons emitted from submerged fuel debris. According to the current estimate, a neutron flux is in the range of 10^2–10^8 n/cm^2/s with a γ-ray dose rate of up to 100 Gy/h, emitted by the widely dispersed ^{137}CS [6]. In order to separate

CONTACT Tetsuichi Kishishita kisisita@post.kek.jp KEK, High Energy Accelerator Research Organization, Institute of Nuclear and Particle Studies, Tsukuba, Ibaraki 305-0801, Japan

This article has been corrected with minor changes. These changes do not impact the academic content of the article.

© 2023 The Author(s). Published by Informa UK Limited, trading as Taylor & Francis Group.
This is an Open Access article distributed under the terms of the Creative Commons Attribution-NonCommercial-NoDerivatives License (http://creativecommons.org/licenses/by-nc-nd/4.0/), which permits non-commercial re-use, distribution, and reproduction in any medium, provided the original work is properly cited, and is not altered, transformed, or built upon in any way. The terms on which this article has been published allow the posting of the Accepted Manuscript in a repository by the author(s) or with their consent.

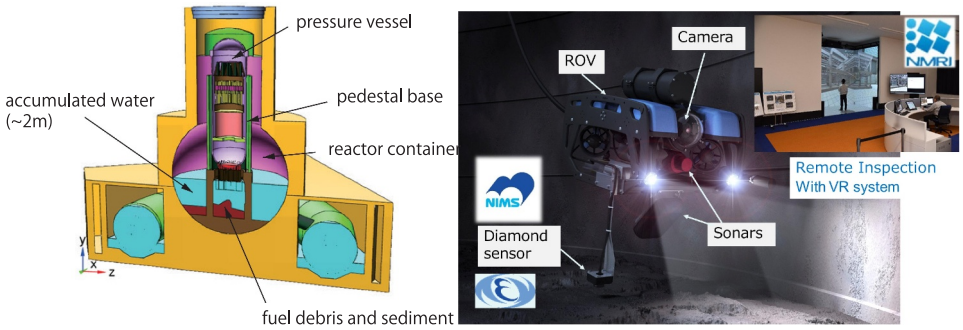

(a) 3D image of the flooded primary containmen vessel at the Fukushima Daiichi NPP

(b) ROV-monitor for remot inspection of the fuel debris.

Figure 1. (a) 3D image of the flooded primary containment vessel at the Fukushima Daiichi NPP and (b) ROV-monitor for remote inspection of the fuel debris.

the rare signals of neutrons associated with the debris from large amounts of background γ-rays, the neutron converters, *e.g.* $^{10}B_4C$ or ^{6}LiF, will be directly coated on the diamond surface. The detector system is installed on the ROV (remotely operated vehicle), as shown in Figure 1 (right). Using the multi-phased array sonar and the acoustic sub-bottom profiling system, the detector system reconstructs the position of the fuel debris in real time.

As a step to realize the diamond-based neutron detectors, we first investigated the device properties of a small scale p-i-n junction diode as a radiation sensor. For processing the charge signals from the sensor, we designed a dedicated readout ASIC in a 65-nm CMOS technology. The primary concern of this article focuses on the feasibility of the prototype system as a radiation sensor. Basic properties of the sensor and specifications of the ASIC are described in Section 2 and 3, respectively. We report on the measurement results in Section 4 and finally give a conclusion in Section 5. The coating methods of neutron converters and the radiation tolerance of the detector will be described elsewhere.

2. Crystal growth and device fabrication

The membrane diamond device was fabricated by applying a recipe of pn junctions in the prototyping facilities at the National Institute for Materials Science in Japan [7]. Homoepitaxial p+, *p*-, *n*-, and n+ layers were grown on a $2 \times 2 \times 0.5$ mm^3 diamond substrate using microwave plasma chemical vapor deposition (MPCVD). The substrate was type-Ib single-crystal diamond {111} synthesized by a high-pressure and high-temperature (HPHT) method. The type-Ib HPHT diamond contains nitrogen with 10^{19} cm^{-3} and exhibits insulating featureS at room temperature. The front and back sideS of the diamond substrate were polished with a crystallographic misorientation angle of 3 degree towards the $[\bar{1}\bar{1}2]$ direction. Prior to be transferred in the MPCVD chamber, the substrate has been cleaned in a boiling acids mixture (HNO_3 and H_2SO_4) at 220°C. The growth of the respective layers was carried out by using four individual MPCVD chambers. The vacuum base pressure was less than 1×10^{-8} Torr before the growth. The temperature of the diamond substrate during the growth has been measured using an optical pyrometer.

The growth conditions of the respective layers are summarized in Table 1. First, the boron (B)-doped p+ layer was grown on the type-Ib diamond substrate. Diborane (B_2H_2) was used as a B source gas. An intrinsic layer (*p*- and *n*- stacked layer) was grown, following the p+ layer growth. Lightly B and phosphorus (P) doping was carried out by the residual impurity in the respective MPCVD chambers. Finally, the heavily P-doped n+ layer was grown on the *n*- layer surface. For heavy P doping, phosphine (PH_3) was used. The crystallinity of the respective homoepitaxial layers was characterized by cross-sectional confocal Raman imaging. The detailed measurement conditions for confocal Raman imaging were described in [8].

Pseudo-vertical p-i-n diodes were formed to obtain diode characteristics on the insulating substrate. Figure 2(a) shows a schematic cross-section of a pseudo-vertical p-i-n diode. The mesa structures were formed using Al mask and inductively coupled plasma (ICP) etching with oxygen gas. The mesa diameter and height were, respectively, 250 μm and 5 μm. After the mesa formation, the conductive graphitic impurity and damage-layer induced by ICP etching were removed by the boiling acids mixture. Ohmic electrodes were formed by electron beam deposition of Ti/Au both on the n+ layer (Mesa-top) and on the p+ layer (Mesa-bottom). The diameter and thickness of ohmic electrodes were 150 μm and 60 nm, respectively. The doping concentrations and the thicknesses of the respective layers were confirmed using secondary mass ion spectrometry (SIMS). The doping concentrations of p+, *p*-, *n*-, and n+ layers were, respectively, [B] 2.0×10^{19} cm^{-3},[B] 3.6×10^{16} cm^{-3}, [P] 2.1×10^{16}cm^{-3}, and [P] 1.0×10^{20} cm^{-3}.

Table 1. Growth conditions of the homoepitaxial p-i-n layers.

Layers	p+	p-	n-	n+
Microwave power [W]	500	1000	500	500
Gas pressure [Torr]	100	140	100	100
CH_4/H_2 [%]	0.08	0.05	0.05	0.05
Impurity gas	B_2H_6	–	–	PH_3
Impurity/carbon [ppm]	B/C, 200	–	–	P/C, 10000
Substrate temperature [°C]	900	1050	900	900

The respective thicknesses of p+, *p*-, *n*-, and n+ layers were 2.0 μm, 2.9 μm, 1.8 μm, and 0.1 μm. Finally, Au wires with a diameter of 30 μm were bonded on ohmic electrodes of four Mesa-tops (n+ layer) and one Mesa-bottom (p+ layer) using a wire-bonding system to connect the readout electronics. Figure 2(b) shows an optical microscope image of the pin diodes after the wire-bonding. Mesa-top and Mesa-bottom were used for the signal output and high voltage application, respectively.

3. Readout ASIC

We chose a 65-nm CMOS technology with a supply rail of 1.2 V, by considering the expected radiation dose of $\approx$ 1 MGy. The chip size is 820 μm $\times$ 1460 μm. The γ-ray rates are calculated to be 1 mega cnt/s $\cdot$ cm^2 with energies below 100 keV, corresponding to 7.7 ke$^-$ as background

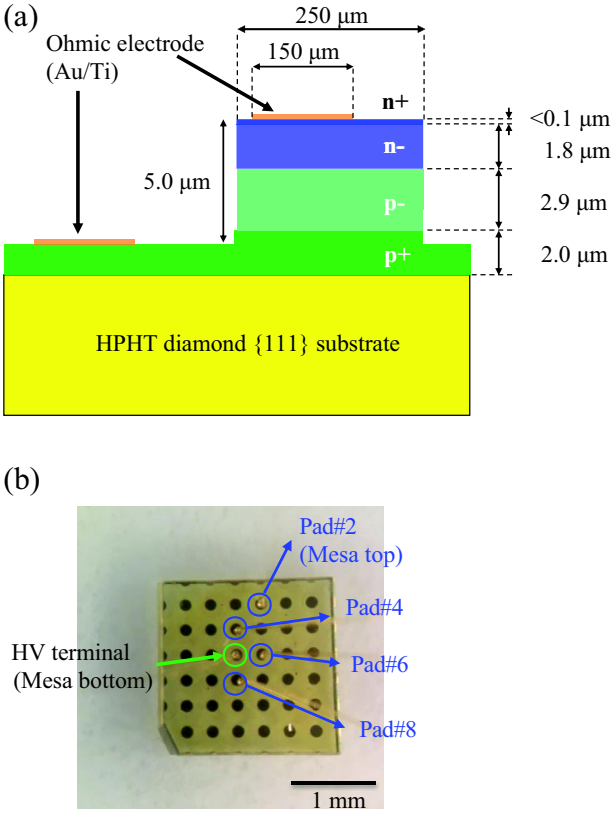

Figure 2. (A) Schematic cross-section of a pseudo-vertical p-i-n diode. (b) Optical microscope image of the p-i-n diodes after the wire-bonding. Mesa-top and -bottom were used for the signal output and high-voltage (HV) application, respectively.

charges, while the main signals from thermal neutrons are $\approx$ 100 ke$^-$ using the ^{10}B neutron converter with an event rate of 100 cnt/s $\cdot$ cm^2. A pulse width of the shaper outputs was thus determined to be $\approx$ 100 ns to minimize the pileups. The power consumption is not a severe constraint in our application.

The chip contains four analog processing chains. Figure 3 shows the block diagram of each channel. The diamond sensor is DC-coupled to an input of the charge-sensitive amplifier (CSA), while test pulses can be injected via an AC-coupling capacitor of 50 fF. The CSA is based on a regulated cascode configuration with a p-channel input transistor ($W/L/M = 5.4\mu\text{m}/500\text{nm}/10$) and $I_d = 200\mu$A. The feedback capacitor C_f was implemented by a metal –insulator–metal structure with a value of 100 fF. A transfer gate type FET was employed for the CSA DC-feedback component. The CSA output is fed into a CR-RC shaping amplifier composed of a pole-zero cancellation circuit and a second-order low-pass filter [9]. The parameters in the shaping amplifier were chosen in the SPICE simulation to achieve the minimum equivalent noise charges at the target input-capacitance of 5 pF, including parasitic components, *e.g.* bonding wire, metal traces, *etc.* The shaper output is fed into two signal paths, one of which is buffered and connected to the output pad. The other signal path is connected to the discriminator, and the hit signals of each channel are sent out in parallel via the LVDS transmitter. Each channel includes 8-bit slow control registers to switch on and off the enable switches and threshold DACs.

4. Measurement results

4.1. Characteristics of the diamond sensor

We first characterized the crystallinity of homoepitaxial p-i-n layers in the diode by cross-sectional Raman imaging. Figure 4 (a) shows the cross-sectional image of the width of the diamond Raman line. The imaging area included the atmosphere and the sample to clear the position of the grown surface. Raman scattering light in the n+ layer could not be detected in the confocal optical system because of the thickness ($< 0.1\mu$m). The cross-sectional image of the line width clearly revealed two boundaries in homoepitaxial p-i-n layers; the *p*- layer/p + layer interface and p+ layer/HPHT diamond substrate

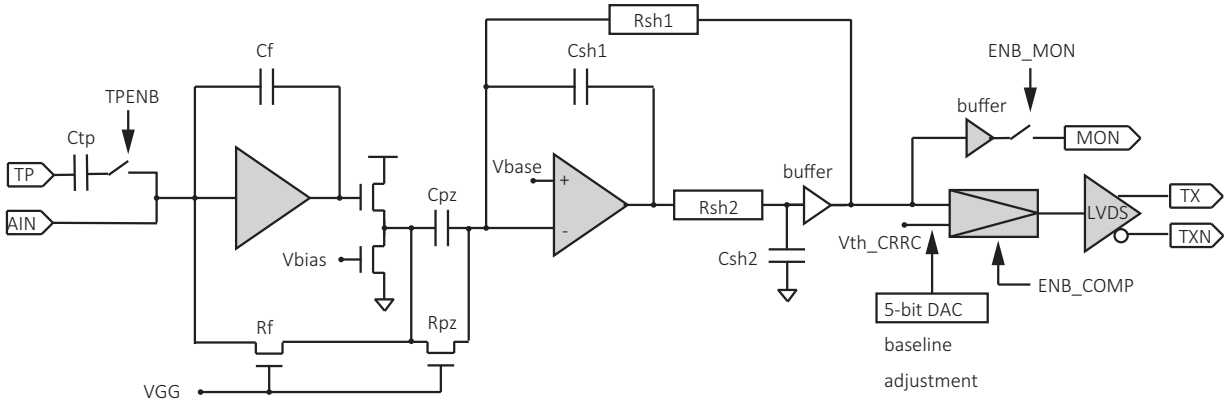

Figure 3. Signal processing chain for each channel. The capacitance values are C_{tp}=50 fF, C_f=C_{pz}=100 fF, C_{sh1}=35 fF, and C_{sh2}=70 fF. The resistance values are as follows: R_{sh1}=2 MΩ, R_{sh2}=150 kΩ, R_f and R_{pz} are within the range of several MΩ adjusted by the gate voltage V_{GG}.

interface. The line widths in the *p*- layer and the *n*- layer were indistinguishable. Histographic analysis has been performed from the obtained image to calculate the average line width in each region. Figure 4 (b) shows the histogram of the line width in Figure 4 (a). The average line width in the p+ layer, the intrinsic layer (*p*- and *n*- stacked layers), and the HPHT substrate were, respectively, 2.05 cm^{-1}, 1.72 cm^{-1}, and 1.86 cm^{-1}.

The width of the Raman line indicates the phonon lifetime of the crystal. The lattice defect in the crystal works as one of the scattering factors of the phonon and increases the width of the Raman line [10]. Candidate lattice defects for the scattering factor include stacking faults, dislocations, and impurities. As the reference [10], the lattice defect with a larger dimension is considered to contribute to the defect scattering of the phonon. Hence, the scattering effect of phonon by point defects (impurities) is less visible in the presence of dislocations and stacking faults. In single-crystal diamond and homoepitaxial films, it has been already reported that the width of the Raman line depends on the boron and nitrogen concentrations in diamond [11,12]. In the case of heteroepitaxial growth where the dislocation density exceeds $10^7 cm^{-2}$, the width depends on the threading dislocation density [13]. In HPHT single-crystal diamond with high B concentrations ($>10^{19} cm^{-3}$), it has been revealed that the combined effect of dislocation and impurity on the width can be evaluated as the distribution of the line width by confocal Raman imaging [14]. In the present results, the cross-sectional image of the width of diamond Raman line indicated the uniform distribution of the width in each layer and substrate. Considering these reports and present result, dislocation in the area with the same impurity type and concentration are considered to be negligibly small, with no effect on uniformity. The difference in the width between each area is considered to be due to the type and concentration of the impurity. Especially, when the impurity concentration exceeds $10^{19} cm^{-3}$, the scattering of the phonon by the impurity

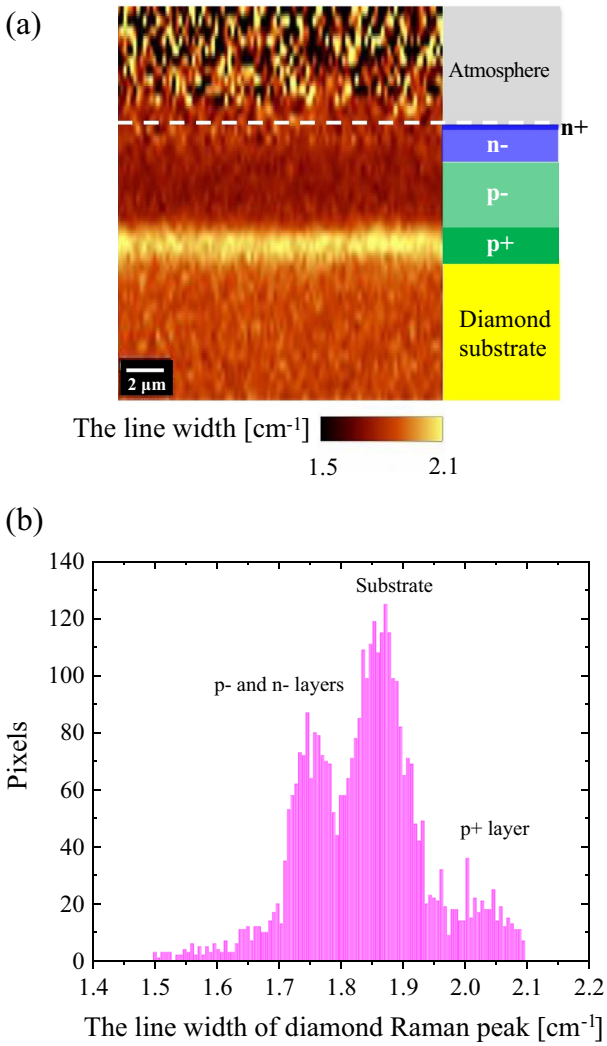

Figure 4. (a) Cross-sectional image of the width of the diamond Raman line. The imaging area included the atmosphere and the sample to clear the position of the grown surface. (b) The histogram of the line width in (a).

could be more pronounced. The scattering of the phonon by B and N impurities could be dominant in the p+ layer and the HPHT substrate, respectively. Figure 4

shows that only point defects can be well controlled in the growth of the diamond pin stacked layer with suppression of extended defects.

Second, we measured the I–V and C–V characteristics of the p-i-n diodes in the atmosphere at room temperature using a microprobe system. A source measure unit (E5280B; Agilent Technologies, Inc.) and an inductance –capacitance–resistance (LCR) meter (4284A; Agilent Technologies, Inc.) were used for the measurements. In both measurements, the reverse voltage was limited to 20 V, which corresponds to the maximum supply voltage of the ROV system, and the applied frequency was 500 Hz in the C-V measurement. Figure 5 (a) presents I–V characteristics of the four p-i-n diodes. The rectification ratio was 10^8 at −20 V. The diodes represented low leakage current less than 10^{-11} A up to −20 V in the atmosphere. High crystallinity in homoepitaxial p-i-n layers can achieve the low leakage current at the reverse voltage. The relevant C–V and $1/C^2$–V curves are presented in Figure 5 (b). We evaluated a net ionized impurity concentration and built-in potential. The net ionized impurity concentration was estimated to be 1.0×10^{16} cm^{-3} from the slope of $1/C^2$ against the voltage around 0 V with a relative dielectric constant of diamond of 5.7. This value is considered to be the net P-donor concentration because the value is consistent with the unintentionally doped P concentration in the n-layer. The built-in potential was deduced to be 4.8 V. The depletion layer thickness deduced from the capacitance was 1.5 μm at −20 V. The $1/C^2$–V characteristic showed a partial depletion of the intrinsic layer at −20 V, and this depletion layer works as the detection layer of the radiation sensor.

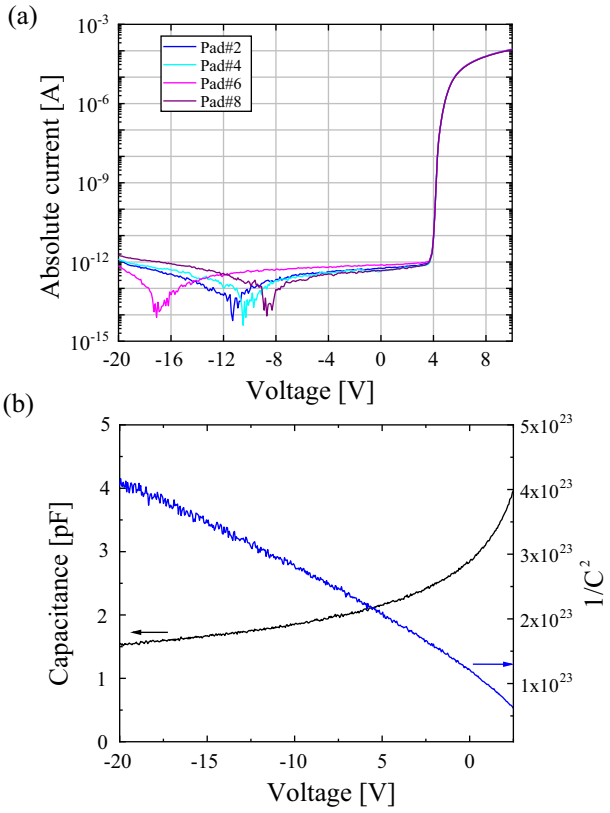

Figure 5. (A) I-V characteristics of the four p-i-n diodes. (b) C-V and $1/C^2$-V curves of the p-i-n diode (Pad#2).

4.2. Characteristic as a radiation detector

Before connecting with the diamond sensor, we evaluated the functions of the ASIC by injecting test pulses and monitored the analog signals. Figure 6 shows the shaper outputs for input charges of $\approx$ 100ke$^-$. The SPICE simulation result is also shown in the same condition. Except the small undershoots presumed to come from the process variation and layout parasitics mainly related in the CR-RC circuit, the peaking time of 80 ns and the voltage gain of 3.2 μV/e$^-$ were well matched with the simulation. Figure 7 shows the measured equivalent noise charges (ENC) as a function of the input capacitance. The difference between the measurement and the SPICE simulation was interpreted as a result of parasitic capacitances of the PCB (printed circuit board) and surface mounted devices. The power consumption was 8 mW per channel.

After the functional test, the diamond sensor and readout ASIC were assembled together on a dedicated PCB. Figure 8 shows the photograph of the PCB. Four channels of the diamond sensor were DC-connected to the inputs of the ASIC via Au wires, and the reverse bias voltages are supplied horizontally from the PCB pad. The bare ASIC die is directly mounted on the PCB and molded on the chip for shielding lights. Then, we irradiated the mono-energetic 5.48 MeV α-particles from ^{241}Am with an intensity of 4.25 kBq inside a vacuum chamber. Due to the limited space on the PCB, the

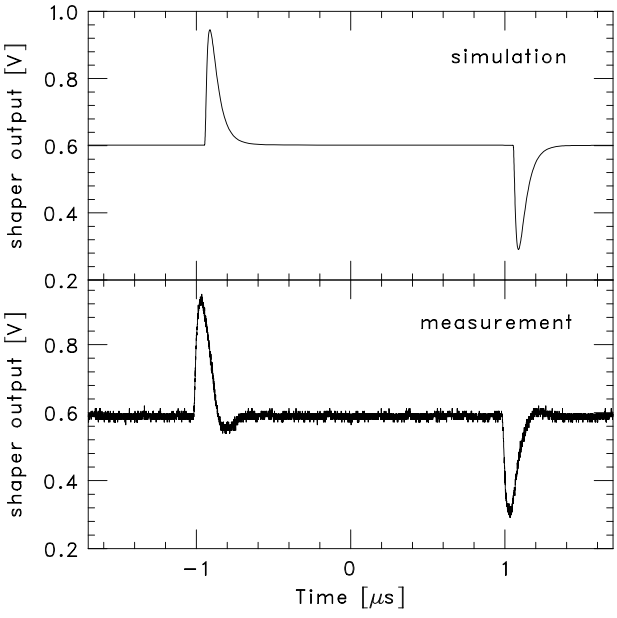

Figure 6. Waveform comparison of the shaper output. A test pulse injects a typical α-particle event which corresponds to $\approx$ 100ke$^-$ into the input.

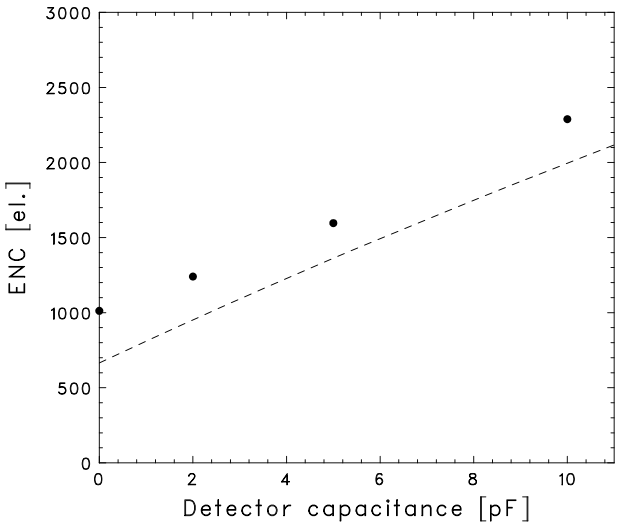

Figure 7. Input capacitance versus equivalent noise charges (ENC). The dashed line indicates the SPICE simulation.

radiation source was located in a 45° diagonal direction to the sensor surface. The outputs of the ASIC were connected to the Multi-Channel Analyzer (MCA-8000D, Amptek).

Figure 9 shows the obtained spectra at room temperature with the reverse bias of 20 V. We calibrated the spectral unit into charges with test pulses. The variation of depletion thickness, due to the partial depletion in the intrinsic layer, is a plausible cause of the variation of peak position. Since the depletion thickness of 1.5 μm is much thinner than a penetration length of 14 μm for the 5.48 MeV α-particles in the diamond, most particles pass through the sensor with partially depositing energies. Although a further study for CCE in the non-depleted layer and substrate should be investigated in the device simulation, we have still plenty of rooms to achieve higher detection efficiency by optimizing the aspect ratio between the size of electrodes and mesa structures. Since thermal neutron events from the boron converter are 100 ke^{-}, we expect the higher charge collection with the current sensor thickness.

The pulse height seemed stable during the exposure for 1 week. The time-dependent CCE caused by the polarization effect is, in general, one of the major limitations of the Schottky barrier diamond sensors. Our device is, however, less sensitive to the metal-diamond surface and free from a charge buildup near electrodes due to its thin crystal volume and inner junction structure.

5. Conclusion

We fabricated a membrane diamond pixel sensor with p-i-n diodes for radiation monitors at the Fukushima NPP in Japan. The pseudo-vertical p-i-n diode structure was formed on the single-crystal diamond {111} substrate by MPCVD and dry-etching process. For reading out signals from the sensor, the dedicated front-end ASIC was developed in a commercial 65-nm CMOS technology. The combined system has demonstrated the multi-channel α-particle detection and thus exploited a new possibility of thermal-neutron imaging using the pixel sensors. The bias dependence of the gain stability is still under investigation; however, the diamond sensor showed a stable behavior for a depletion thickness of 1.5 μm with the reverse bias of 20 V. As the next step, we will investigate effective coating methods of the neutron converters on the the diamond surface. Along with the process iterations for higher detection efficiency, we plan to install this prototype system on board the ROV, which is currently under development by Japan-UK collaboration, and its demonstration tests will be conducted in a PCV mock-up water tank. Such a compact and rad-hard radiation detector also has a great impact as a radiologically diagnostic tool at the high-intensity and high-energy accelerator facilities.

Acknowledgments

This study was carried out as "Research and Development of Radiation-resistant Sensor for Fuel Debris by Integrating Advanced Measurement Technologies (30I123)" in the framework of FY2018 FY2020 Center of World Intelligence Project for Nuclear Science/Technology and Human Resource Development and partially funded by CLADS, JAEA. This work was also supported by KAKENHI Grant-in-Aids (22H01255) for publication.

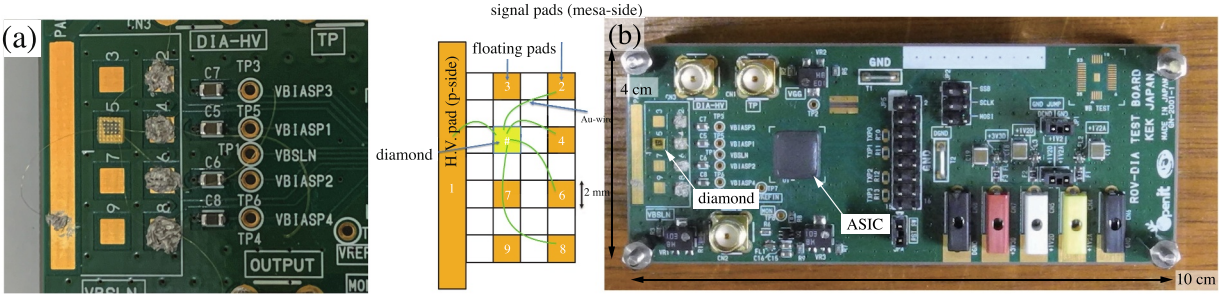

Figure 8. (a) Close up image of the diamond sensor and connection to the PCB. (b) Photograph of the dedicated PCB. The readout ASIC was directly mounted on the PCB and molded after wire-bonding.

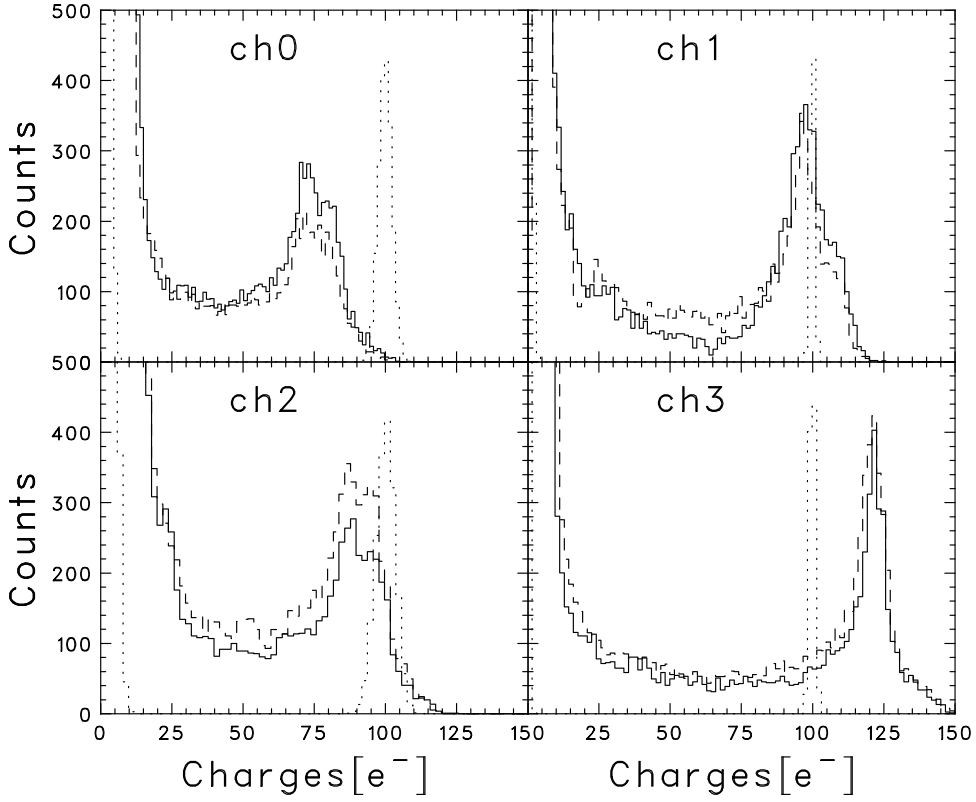

Figure 9. Radiation spectra obtained by irradiating 5.48 MeV α-particles from ^{241}AM. The reverse voltage of −20 V was applied to the p-side of the membrane diamond sensor. The solid and dashed lines indicate the spectra, which were obtained soon after the reverse biasing and after 1 week, respectively. Each exposure time was 20 min. The dotted lines indicate the pedestal and test pulse spectra injected via an on-chip capacitance.

Disclosure statement

No potential conflict of interest was reported by the authors.

ORCID

Tetsuichi Kishishita http://orcid.org/0000-0001-9694-6121
Kimiyoshi Ichikawa http://orcid.org/0000-0002-8655-3516
Masayuki Hagiwara http://orcid.org/0000-0003-0236-2905

References

[1] Kaneko JH, Tanaka T, Imai T, et al. Radiation detector made of a diamond single crystal grown by a chemical vapor deposition method. Nucl. Instrum. Methods. Phys. Res A. 2003;505(1–2):187. DOI:10.1016/S0168-9002(03)01048-9
[2] Almaviva S, Marinelli M, Milani E, et al. Chemical vapor deposition diamond based multilayered radiation detector: physical analysis of detection properties. J. Appl. Phys. 2010;107(1):014511. DOI:10.1063/1.3275501
[3] Pomorski M, Caylar B, Bergonzo P. Super-thin single crystal diamond membrane radiation detectors. Appl. Phys. Lett. 2013;103(11):112106.
[4] Holmes J, Dutta M, Koeck FA, et al. A 4.5μm PIN diamond diode for detecting slow neutrons. Nucl. Instr. Meth A. 2018;903:297.
[5] https://www.tepco.co.jp/en/decommision/index-e.html
[6] Riyana ES, Okumura K, Terashima K. Calculation of gamma and neutron emission characteristics emitted from fuel debris of Fukushima Daiichi nuclear power station. J. Nucl. Sci. Technol. 2019;56(9–10):922.
[7] Koizumi S, Watanabe K, Hasegawa M et al. Ultraviolet emission from a diamond pn junction. Science. 2001;292(5523):1899.
[8] Ichikawa K, Shimaoka T, Kato Y et al. Dislocations in chemical vapor deposition diamond layer detected by confocal Raman imaging. J. Appl. Phys. 2020;128(15):155302.
[9] Kishishita T, Sato G, Ikeda H, et al. Low-noise analog ASIC for silicon and CdTe sensors. IEEE Trans. Nucl. Sci. 2010;57(5):2971. DOI:10.1109/TNS.2010.2063038
[10] Falkovsky LA. Width of optical phonons: influence of defects of various geometry. Phys. Rev B - Condens. Matter. Mater. Phys. 2001;64(2):024301.
[11] Faggio G, Messina G, Santangelo S et al. Raman scattering in boron-doped single-crystal diamond used to fabricate Schottky diode detectors. Jorn. Quant. Spectrosc. Radiat. Transf. 2012;113(18):2476.
[12] Surovtsev NV, Kupriyanov IN. Effect of nitrogen impurities on the Raman line width in diamond, revisited. Crystals. 2017;7(8):239.
[13] Stehl C, Fischer M, Gsell S et al. Efficiency of dislocation density reduction during heteroepitaxial growth of diamond for detector applications. Appl. Phys. Lett. 2013;103(15):151905.
[14] Srimongkon K, Ohmagari S, Kato Y et al. Boron inhomogeneity ofHPHT-grown single-crystal diamond substrates: confocal micro-Raman mapping investigations. Diam. Relat. Mater. 2016;63:21–25.